AD-A105 749 NAVAL RESEARCH LAB WASHINGTON DC F/G 9/3
MICROWAVE ENERGY DEPOSITION, BREAKDOWN AND HEATING OF NITROGEN --ETC(U)
OCT 81 C L YEE, A W ALI
UNCLASSIFIED NRL-MR-4617 NL

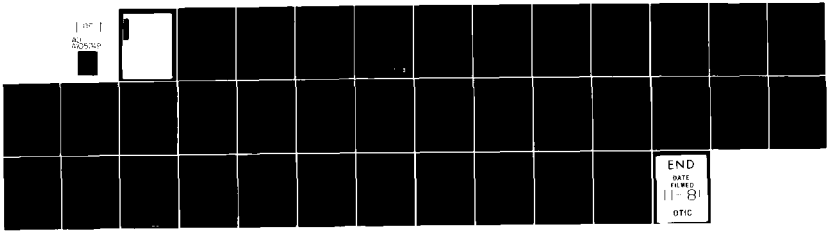

SECURITY CLASSIFICATION OF THIS PAGE (When Data Entered)

REPORT DOCUMENTATION PAGE

READ INSTRUCTIONS BEFORE COMPLETING FORM

1. REPORT NUMBER: NRL Memorandum Report 4617	2. GOVT ACCESSION NO.: AD-A105 749
3. RECIPIENT'S CATALOG NUMBER	
4. TITLE (and Subtitle): MICROWAVE ENERGY DEPOSITION, BREAKDOWN AND HEATING OF NITROGEN AND AIR	5. TYPE OF REPORT & PERIOD COVERED: Interim report on a continuing NRL problem.
	6. PERFORMING ORG. REPORT NUMBER
7. AUTHOR(s): C. L. Yee and A. W. Ali	8. CONTRACT OR GRANT NUMBER(s)
9. PERFORMING ORGANIZATION NAME AND ADDRESS: Naval Research Laboratory, Washington, DC 20375	10. PROGRAM ELEMENT, PROJECT, TASK AREA & WORK UNIT NUMBERS: 62734N; 80-WF-34-388-501; 47-0868-0-1
11. CONTROLLING OFFICE NAME AND ADDRESS: Naval Air Systems Command, Washington, DC 20361	12. REPORT DATE: October 16, 1981
	13. NUMBER OF PAGES: 36
14. MONITORING AGENCY NAME & ADDRESS(if different from Controlling Office)	15. SECURITY CLASS. (of this report): UNCLASSIFIED
	15a. DECLASSIFICATION/DOWNGRADING SCHEDULE

16. DISTRIBUTION STATEMENT (of this Report)

Approved for public release; distribution unlimited.

17. DISTRIBUTION STATEMENT (of the abstract entered in Block 20, if different from Report)

18. SUPPLEMENTARY NOTES

*Present address: Mission Research Corporation, Alexandria, VA 22312

19. KEY WORDS (Continue on reverse side if necessary and identify by block number)

Microwave
Absorption
Reflection
N_2 Breakdown
Air breakdown

20. ABSTRACT (Continue on reverse side if necessary and identify by block number)

A comprehensive code is developed for the microwave energy deposition in N_2 to describe the breakdown and heating of nitrogen. The microwave absorption and reflection from a nitrogen plasma is based on wave optics. The ionization and the deionization of N_2, however, is described in detail by an N_2 chemistry code (CHEM-N_2) which pro-

(Continues)

DD FORM 1 JAN 73 1473 EDITION OF 1 NOV 65 IS OBSOLETE
S/N 0102-014-6601

SECURITY CLASSIFICATION OF THIS PAGE (When Data Entered)

20. ABSTRACT (Continued)
vides plasma diagnostics capabilities by calculating emission intensities of the second positive and the first negative band systems of N_2^2 and N_2^{+}.

The code is applied to breakdown calculations in $N_2^{'}$ and the results are in reasonable accord with experimental data. The wave optics code for energy deposition is also coupled to an air chemistry code (CHMAIR) to describe the breakdown off a reflecting surface.

An insight is provided into the plasma absorption by using a simple slab density profile for the electrons. This models roughly the profile expected in air breakdown off a reflecting surface. Simulation results show a steep localized electron density profile at the interference maximum. These simple calculations show the plasma reflectivity to be small (< 25%) for 1 cm light at high electron densities, N_e 10^{15} $cm^{-3} \gg N_c = 10^{13}$ cm^{-3}. Simulation results also show the possibility of attaining high electron density. However, in breakdown off a reflecting surface, the microwave is decoupled from the plasma when the absorption length is less than one-half the wavelength of the light. Important questions to be addressed in the future include the possibility of plasma maintenance, gas heating, shock formation, plasma decoupling and effects of strong nonlinear forces.

CONTENTS

MICROWAVE ENERGY DEPOSITION, BREAKDOWN AND HEATING OF NITROGEN AND AIR

I. INTRODUCTION

The interactions of the high power microwave radiation with air, matter and plasmas have potential for various applications, and hence merit detailed studies and analysis. A detailed study, theoretical and experimental, is necessary in order to delineate possible regimes for applications purposes.

Studies can be performed analytically to provide answers in the limiting cases. However, the phenomena of the microwave interaction with air, matter and plasmas are complex and require time and space dependent treatments of a large number of physical processes. This can be carried out in a self consistent manner by developing detailed computer codes which treat part or all the phenomena.

This report deals with and describes computer codes, developed at NRL, for the analysis of the pulsed microwave interaction with nitrogen (N_2). The interaction is considered from the first principles with the microwave absorption by one or few free electrons, present in the gas, the electron build up, the breakdown, and the microwave absorption and reflection by the plasma electrons. The computer code which describes this phenomena is basically, consists of two codes coupled together. One, describes the electromagnetic radiation (E and M Code) and the other describes the physics and chemistry of the ionization and the deionization in N_2 (CHEM-N_2) Code. The E and M Code, however, can also be coupled into an air chemistry code to describe the breakdown in air, as discussed in the report.

Manuscript submitted July 24, 1981.

In Section 1 the E and M Code and the solution of the wave equation is described. Section 2 gives the description of the pure N_2 chemistry code, and Section 3 deals with the breakdown calculations in N_2, where the breakdown power thresholds are compared with experimental data for several nitrogen pressures. In Section 4, the E and M Code coupled to an air chemistry code is utilized to calculate breakdown in air near a surface. For air breakdown near a surface one can utilize microwave powers below the threshold for air breakdown by a factor of 4 and still be able to break down the air. This is due to the fact that the microwave reflection from the surface interferes constructively with the outgoing wave resulting in doubling the electric field at a distance of $\frac{\lambda}{4}$ from the surface.

2. The E and M CODE

In order to describe the microwave absorption by a plasma one must know the electric field at all positions in the plasma. To do this we consider the solution of one dimensional wave equation[1]

$$\frac{\partial^2 E_z}{\partial t^2} + \nu_c \frac{\omega_p^2}{\omega^2 + \nu_c^2} \frac{\partial E_z}{\partial t} - c^2 \frac{\partial^2 E_z}{\partial z^2} + \omega_p^2 \frac{\omega^2}{\omega^2 + \nu_c^2} E_z = 0 \quad (1)$$

for a plane wave incident normal to a plasma. The electron neutral (electron-ion) collision frequency is denoted by ν_c and the plasma frequency is defined as $\omega_p^2 = \frac{4\pi e^2 N_e}{m}$ where the notation is standard. Since the absorption length at microwave frequency is long at the critical density $N_c \equiv m\omega^2/4\pi e^2$ we can specify an essentially free-space boundary condition[2] for the incoming light as

$$\frac{\partial E_z}{\partial t} - c \frac{\partial E_z}{\partial y} = 2 \frac{\partial}{\partial t} U_{in} \quad (2)$$

where U_{in} is the amplitude of the known incident light. This boundary condition is also applicable to a plasma-vacuum interface as constructed in experiments using a mylar divider. The right side boundary condition in the plasmas specified as

$$\frac{\partial E_z}{\partial t} - c \frac{\partial E_z}{\partial y} = -4\pi j$$

where $j = \sigma E_z = \frac{\nu_c}{4\pi} \frac{\omega_p^2}{\omega^2 + \nu_c^2} E_z$. Again for low densities, the right hand side of equation (2) is similar to a free-space propagating to the right. Equation (1) is differenced implicitly to retain stability for large times steps in a high density plasma, $\omega_p^2 \gg \nu_c^2 + \omega^2$. The implicit difference form of equation (1) is

$$\frac{E_j^{n+1} - 2E_j^n + E_j^{n-1}}{(\Delta t)^2} + \frac{\nu_c}{2} \frac{\omega_p^2}{\omega^2 + \nu_c^2} \frac{E_j^{n+1} - E_j^{n-1}}{\Delta t} -$$

$$\frac{c^2}{4} \frac{(\delta^2 E)_j^{n+1} + 2(\delta^2 E)_j^n + (\delta^2 E)_j^{n-1}}{(\Delta y)^2} + \omega_p^2 \frac{\omega^2}{\omega^2 + \nu_c^2} = 0 \qquad (3)$$

where $(\delta^2 E)_j^n \equiv E_{j+1}^n - 2E_j^n + E_{j-1}^n$. This can also be cast into a tri-diagonal system of the form

$$-\beta^2 E_{j+1}^{n+1} + (1 + \gamma + 2\beta^2) E_j^{n+1} - \beta^2 E_{j-1}^{n+1} = (2 - \omega_p^2 \Delta t^2 - 4\beta^2) E_j^n$$

$$+ 2\beta^2 E_{j-1}^n + \beta^2 E_{j+1}^{n-1} - (1 - \gamma + 2\beta^2) E_j^{n-1} + \beta^2 E_{j-1}^{n-1} = D_j^n \qquad (4)$$

where $\beta = \frac{\Delta t}{2\Delta y}$ and $\gamma = \frac{\nu_c}{2} \frac{\omega_p^2}{\omega^2 + \nu_c^2}$ A solution of a tri-diagonal system of equations[3]

$$-A_j E_{j+1}^{n+1} + B_j E_j^{n+1} - C_j E_{j-1}^{n+1} = D_j^n$$

can be shown to be

$$E_{j+1}^{n+1} = G_{j+1}^{n+1} E_j^{n+1} + F_{j+1}^{n+1}$$

where the G_j's and F_j's satisfy the recursion relation

$$G_j^{n+1} = \frac{C_j}{B_j - A_j G_{j+1}^{n+1}} \quad \text{and} \quad F_j^{n+1} = \frac{D_j + A_j F_{j+1}^{n+1}}{B_j - A_j G_{j+1}^{n+1}} \; . \tag{5}$$

The solution technique is then to specify the boundary condition and sweep the mesh space for the G_j's and F_j's. After which we sweep again to obtain the updated electric field.

The stability analysis of the implicit scheme can be made simple by dropping the last term of Equation (1). This term is typically not important in determining the stability criterion. We rewrite Equation (1) without this term as a system of two coupled equations.

$$\frac{\partial V}{\partial t} = \nu_c \frac{\omega_p^2}{\omega^2 + \nu_c^2} V + \frac{\partial W}{\partial y} \tag{6}$$

$$\frac{\partial W}{\partial t} = \frac{\partial V}{\partial y} \tag{7}$$

where $V = \frac{\partial E_z}{\partial t}$ and $W = \frac{\partial E_z}{\partial y}$. Choosing an arbitrary fourier component we let $V_j^n = \xi^n \exp(-ikj\Delta y)$ and $W_j^n = \rho^n \exp(-ikj\Delta y)$.

We find after some algebra that

$$\begin{pmatrix} \xi \\ \rho \end{pmatrix}^{n+1} = \frac{1}{1 + \alpha^2 + \gamma^2} \begin{pmatrix} 1 - \gamma - \alpha^2 & 2i\alpha \\ 2i\alpha & 1 + \gamma - \alpha^2 \end{pmatrix} \begin{pmatrix} \xi \\ \rho \end{pmatrix} = A \begin{pmatrix} \xi \\ \rho \end{pmatrix}^n \tag{8}$$

where $\alpha \equiv \frac{c\Delta t \sin(k\Delta y/2)}{\Delta y}$. Stability requires the eigenvalues of the amplification matrix A to be less than or equal to 1. One can show that the eigenvalues are bounded by

$$|\lambda^{\pm}| = \frac{1 - \gamma + \alpha^2}{1 + \gamma + \alpha^2} \leq 1 \qquad (9)$$

and hence the implicit scheme is unconditionally stable for arbitrary α.

The boundary conditions are explicitly differenced and are coupled to an explicit form of Equation (1) to obtain boundary value. This explicit form of Equation (1) is:

$$\frac{E_j^{n+1} - 2E_j^n + E_j^{n-1}}{(\Delta t)^2} + \frac{\nu_c}{2} \frac{\omega_p^2}{\omega^2 + \nu_c^2} \frac{E_j^{n+1} - E_j^{n-1}}{\Delta t}$$

$$-c^2 \frac{E_{j+1}^n - 2E_j^n + E_{j-1}^n}{(\Delta y)^2} + \omega_p^2 \frac{\omega^2}{\omega^2 + \nu_c^2} E_j = 0 \qquad (10)$$

Once the boundary values are obtained, we use the implicit difference equation for all interior points. The boundary values are used as "first" values in sweeping the tri-diagonal system of equation. Since locally the explicit differencing is stable for

$$(\Delta t^2) \left[\left(\frac{c}{\Delta y}\right)^2 + \tfrac{1}{4}\left(\nu_c \frac{\omega_p^2}{\omega^2 + \nu_c^2}\right)^2 \right] \leq 1$$

the boundary must be at low density to maintain stability, $\omega_p^2 \leq \nu_c^2 + \omega^2$.

In practice, the implicit scheme must satisfy the explicit stability criterion to maintain accuracy and minimum phase error. In considering microwave breakdown off a reflecting surface, this is important since the interference maximum determines the breakdown field.

As a check on the code, we perform simulations, on free-space, propagation and reflection off metal surface in a vacuum. Figure (1a) shows the reflected light for a propagating electromagnetic wave in vacuum for a single pass to the reflecting surface and back to the point of entry of the radiation. The system length is $kL = 15$ (where $k = 2\pi/\lambda$) so the return time of the radiation is $t_R\omega = 30$ for $c\Delta t = 0.9\Delta y$. The code tracks the propagation velocity well, however, in the transient time $\omega t \leq 30$, the numerics has introduced errors in the reflected wave. The average reflected wave should be zero during the transient period, yet we see the average reflected wave of roughly 10% of the incident light. Figure (1b) shows the spatial electric field (in normalized variables). Since the launched incoming wave is unity, the combined wave once reflected from the surface should be of amplitude two. We see the implicit scheme has introduced large errors in the phase of the wave and therefore the reconstructed wave. Figure (2a) shows a similar test with a reduced time step $c\Delta t = 0.2\Delta y$. However, in this test, the reflected wave in the transient period is less than 1% of the incident light. The smaller phase error reconstructs the interference patterns to its proper maximum of two as can be seen in Figure (2b). An extensive parameter study shows good results are obtained using the implicit scheme for $c\Delta t \leq 0.2\Delta y$.

Also as a check, we consider light normally incident on a linear density profile. The density profile in this collisionless plasma ($\nu_c = 0.1\omega$) rises from zero to the cut off density N_c with a density scale length of $kL_s = 10$. The Airy function solution requires standing wave pattern toward the incident light and evanescent wave in the overdense plasma. Figure (3) shows the solution obtained for the electric field using the implicit scheme with the boundary conditions. Analytic solution shows the computed field is accurate in location of the first large maximum, the amplitude of the reflected light and the amplitude of the largest maximum. The various test problems thus confirm the validity of the code.

3. N_2 BREAKDOWN AND OPTICAL DIAGNOSTICS

To describe the nitrogen breakdown by the microwave radiation, we have

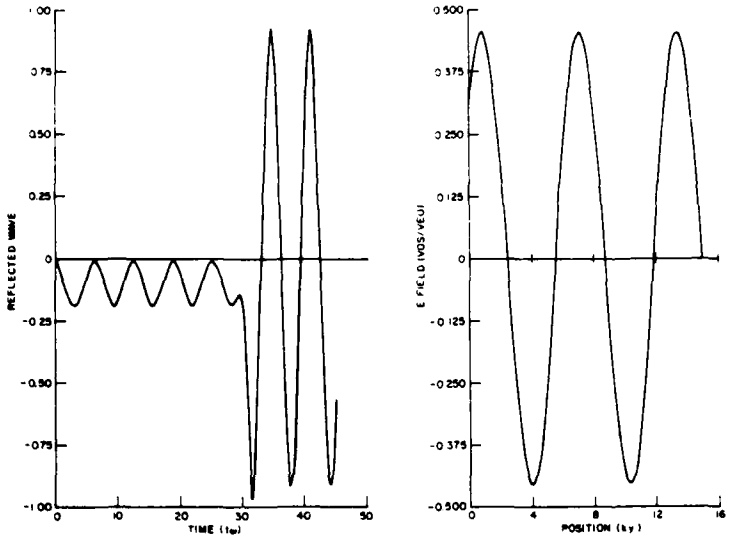

(a) (b)

Fig. 1 — Test run with $c\Delta t = 0.9\Delta y$ for a plane wave reflected from a surface (a) reflected wave (VOS/VEO) versus time ($t\omega$) and (b) electric field (VOS/VEO) versus position (ky) where VOS and VEO indicate the oscillatory and the thermal velocities of the electron, respectively.

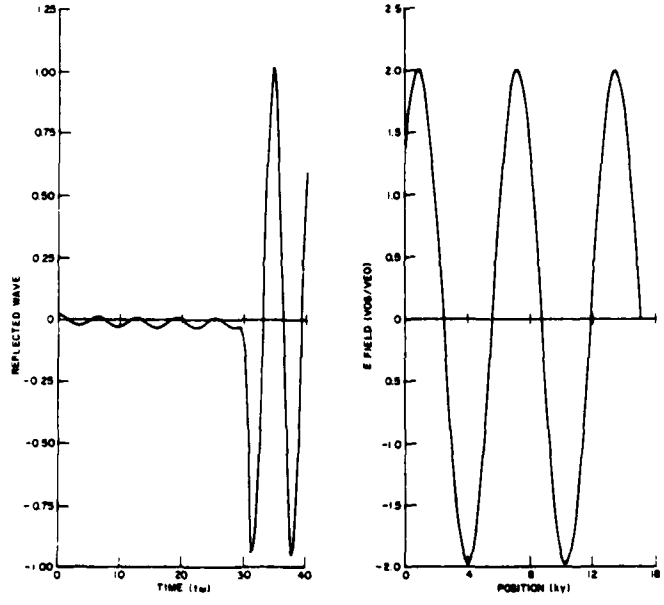

(a) (b)

Fig. 2 — Test run with $c\Delta t = 0.2\Delta y$ for a plane wave reflected from a surface (a) reflected wave (VOS/VEO) versus time ($t\omega$) and (b) electric field (VOS/VEO) versus position (ky) where VOS and VEO indicate the oscillatory and the thermal velocities of the electron, respectively.

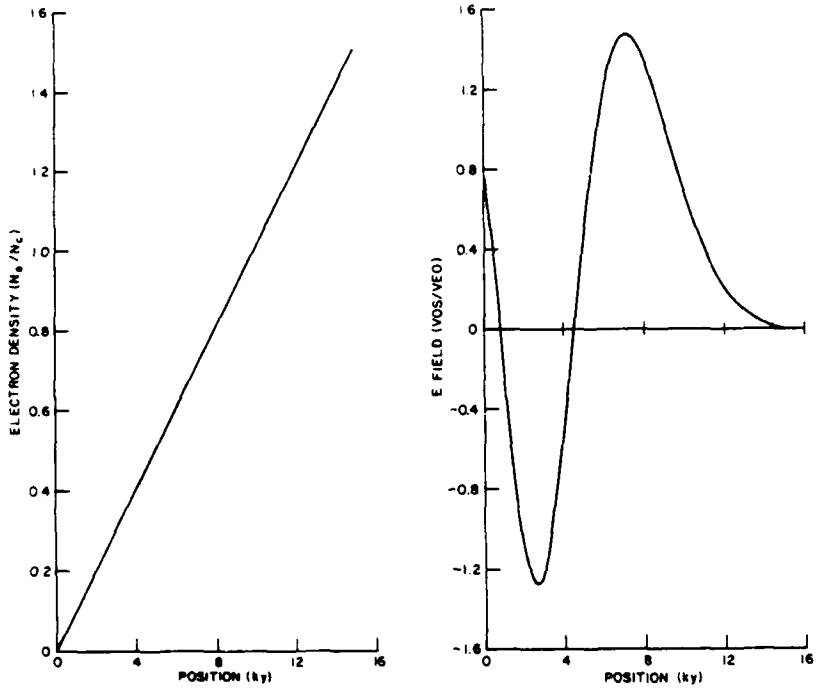

(a) (b)

Fig. 3 — Test run for a plane wave normally incident on a linear plasma profile. The graph shows the electric field (VOS/VEO) versus position (ky).

developed an N_2 chemistry code. The code calculates the time developments of $N_2^+(x)$, $N_2^+(B)$, N_4^+, N, $N(^2D)$, $N_2(A^3\Sigma)$, $N_2(B^3\pi)$, $N_2(C^3\pi)$, N_e, T_e, T_v, and T_g, where the last three symbols designate the electron, the N_2 - vibrational and the gas temperatures, respectively. The purpose for the calculation of the population densities of several excited states is to provide volume emission rates for optical diagnostics of the plasma and the investigation of the ionization from the excited states.

3.1 N_2 CHEMISTRY

A free electron gains energy, in the field of the microwave radiation, it undergoes both elastic and inelastic collisions with N_2, thereby losing part or all of the energy gained from the field. When the electron energy reaches and overshoots the ionization threshold for N_2 an ionization event may occur according to reaction (11).

$$e + N_2 \rightarrow N_2^+ + 2e \tag{11}$$

Higher energy electrons could ionize N through the dissociative ionization. However, the threshold for this process is higher by $\sim$ 10 eV compared to that for reaction (11). Therefore, process (11) is the predominant reaction for the breakdown ionization by microwave radiation.

The deionization of the plasma occurs primarily through the dissociative recombination of the nitrogen ion N_2^+ and its cluster ion N_4^+, i.e.,

$$N_2^+ + e \rightarrow N + N \tag{12}$$

$$N_4^+ + e \rightarrow N_2 + N_2 \tag{13}$$

The N_4^+ cluster forms via a three-body process [4,5] i.e.,

$$N_2^+ + N_2 + N_2 \rightarrow N_4^+ + N_2 \tag{14}$$

and is obviously important at atmospheric pressures and lower gas temperatures. When the gas temperature rises, however, the formation of N_4^+ is inhibited by the slowing down of the forward reaction in (14) and by the collisional breakup of N_4^+ (i.e., the reverse reaction of (14) becomes operative.

The deionization also proceeds via the three-body collisional recombination, however, it may become important after breakdown and when the electron density is quite high. Finally, the electron loss occurs also through diffusion.

3.2 ELECTRON ENERGY GAIN AND LOSS PROCESSES IN N_2

The electron energy loss processes in N_2 proceed by the elastic and inelastic collisions. The energy loss by elastic collisions is dependent on ν_c, where ν_c is the momentum transfer collision frequency. The collision frequency depends on the electron energy (temperature) and the momentum transfer cross section. The cross section[6] is shown as a function of the electron energy in Figure (4). By folding this cross section with the appropriate electron velocity distribution, one obtains the momentum transfer collision frequency. Thus the rate of the energy loss by an electron through the elastic collisions can be expressed as

$$R_e = \frac{2m}{M} \nu_c \left(\frac{3}{2} T_e - \frac{3}{2} T_g\right) \tag{15}$$

where m is the electron mass and M is the mass of the nitrogen molecule.

The electron inelastic energy loss processes in N_2 are the excitation, the dissociation and the ionization of the nitrogen molecule. These processes are expressed as

$$e + N_2 \rightarrow N_2^{\ddagger} + e \tag{16}$$

$$e + N_2 \rightarrow N_2^{*} + e \tag{17}$$

$$e + N_2 \rightarrow N + N + e \tag{18}$$

in addition to Equation (1). Equation (16) indicates the excitations of the N_2 ground state vibrational levels, while Equation (17) represents the excitations of the electronic states of N_2. The N_2 electronic states include the triplets and the singlets whose cross sections are presented and discussed elsewhere.[7] The cross section for the N_2 disassociation, however, is a composite of a large number of singlet states which predissociate. Thus, the energy loss by electrons in N_2 can be summed up to include the losses due to the excitations of the ground state vibrational levels, the excitation of

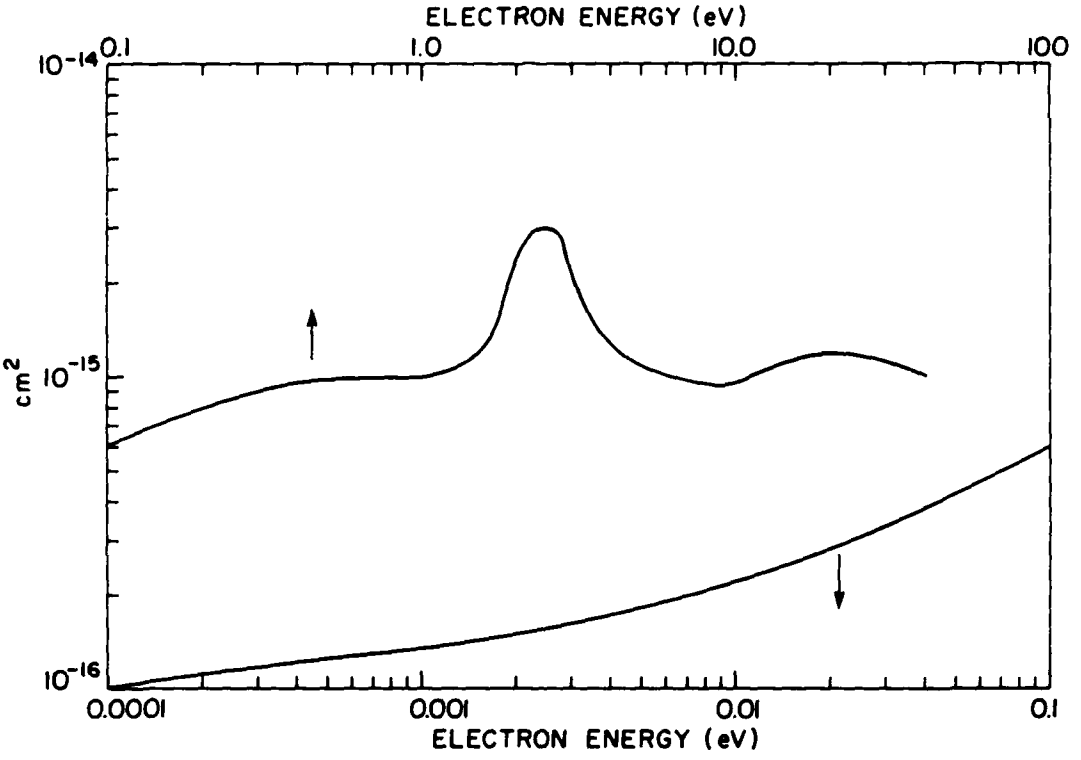

Fig. 4 — The Electron Momentum Transfer cross section in nitrogen (N_2)

the electronic states $A^2\varepsilon$, $B^3\varepsilon$, $C^3\pi$, $a^1\pi$, the dissociation, and the ionization of N_2.

Briefly, the vibrational cross sections are from the measurements of Schulz[8] and are well established as to the peak of the total and the shape of the individual cross sections[8-10]. The cross section for the ionization is from the measurement of Rapp and Golden[11] and the cross section for the dissociation is from the measurements of Winters[12] and Zipf and Mclaughlin[13]. The cross section for the triplet states are discussed in the next section.

The rate coefficients for all the inelastic processes discussed above have been obtained[14, 15] for a Maxwellian electron velocity distribution and are utilized in the breakdown code. Thus, if one designates x_i as the electron impact rate-coefficient for the excitation of the ith state whose excitation energy is E_i, the rate of the electron energy loss in N_2 can be expressed as

$$R_{in} = \Sigma_i \; x_i \; E_i \; N_2$$

Where the summation is over eight ground state vibrational levels, the singlet and triplet electronic states, the dissociation and the ionization of N_2. A similar equation for the energy loss in the nitrogen atom can be utilized, with the appropriate rate coefficients.

Other electron energy loss processes are the excitation of the excited states from a lower state (not the ground state) and the ionization of the excited states.

The energy gain mechanisms for an electron are the energy absorption from the field of the microwave i.e., the inverse bremsstrahlung, the electron impact deexcitation of the ground state vibrational levels and the deexcitation of the electronic states of the N_2 molecule and the nitrogen atom.

3.3 EXCITED STATES

The code as indicated earlier calculates the time histories of several excited states of N_2 which are discussed below.

$A^3\Sigma$: The $A^3\Sigma$ state is a metastable and has a life time of 1 sec and an

excitation[16] energy of 6.1 eV. Its excitation cross section by electron impact has been measured and calculated by several investigators which are discussed in Ref (7), and shown in Figure 5. The electron impact ionization of the $A^3\Sigma$ state has been calculated bu Kukulin, et al.[17] The excitation energy of the $A^3\Sigma$ state generally ends up as a heating source for the gas because of the rapid quenching of the state by the atomic nitrogen. The rate coefficient for the quenching[16] of the $A^3\Sigma$ by N is 5×10^{-11} cm^3/sec.

$B^3\Sigma$: The $B^3\Sigma$ state is excited, from the ground state of N_2, by electron impact, has an excitation energy[16] of 7.2 eV, and is the upper level for the first positive band system, ($B^3\pi \rightarrow A^3\pi$). The strong vibrational bands of this system[18] are given in Table 1.

TABLE 1

Relatively Strong Emissions in the First Positive Band System

Wave length (Å)	Transition (ν', ν'')	Wavelength (Å)	Transition (ν', ν'')
7503	4, 2	6069	6, 2
6704	5, 2	6013	7, 3
6623	6, 3	5959	8, 4
6544	7, 4	5906	9, 5
6468	8, 5	5854	10, 6
6394	9, 6	5804	11, 7
6322	10, 7	5755	12, 8

The life times of these transitions are in the range of 10^{-5} sec to 10^{-6} sec and are quenched[19] by N_2 with a rate coefficient of $\sim$ (1-2) x 10^{-11} cm^3/sec.

The electron impact excitation cross section for the $B^3\pi$ state have been measured and calculated by numerous investigators[7] and some of these are shown in Figure 6.

$C^3\pi$: The $C^3\pi$ state is excited from the ground state of N_2, by electron impact has an excitation energy[16] of 11 eV and is the upper level for the second positive band systems, ($C^3\pi \rightarrow B^3\pi$). Some of the strong[18] bands of this system are given in Table 2.

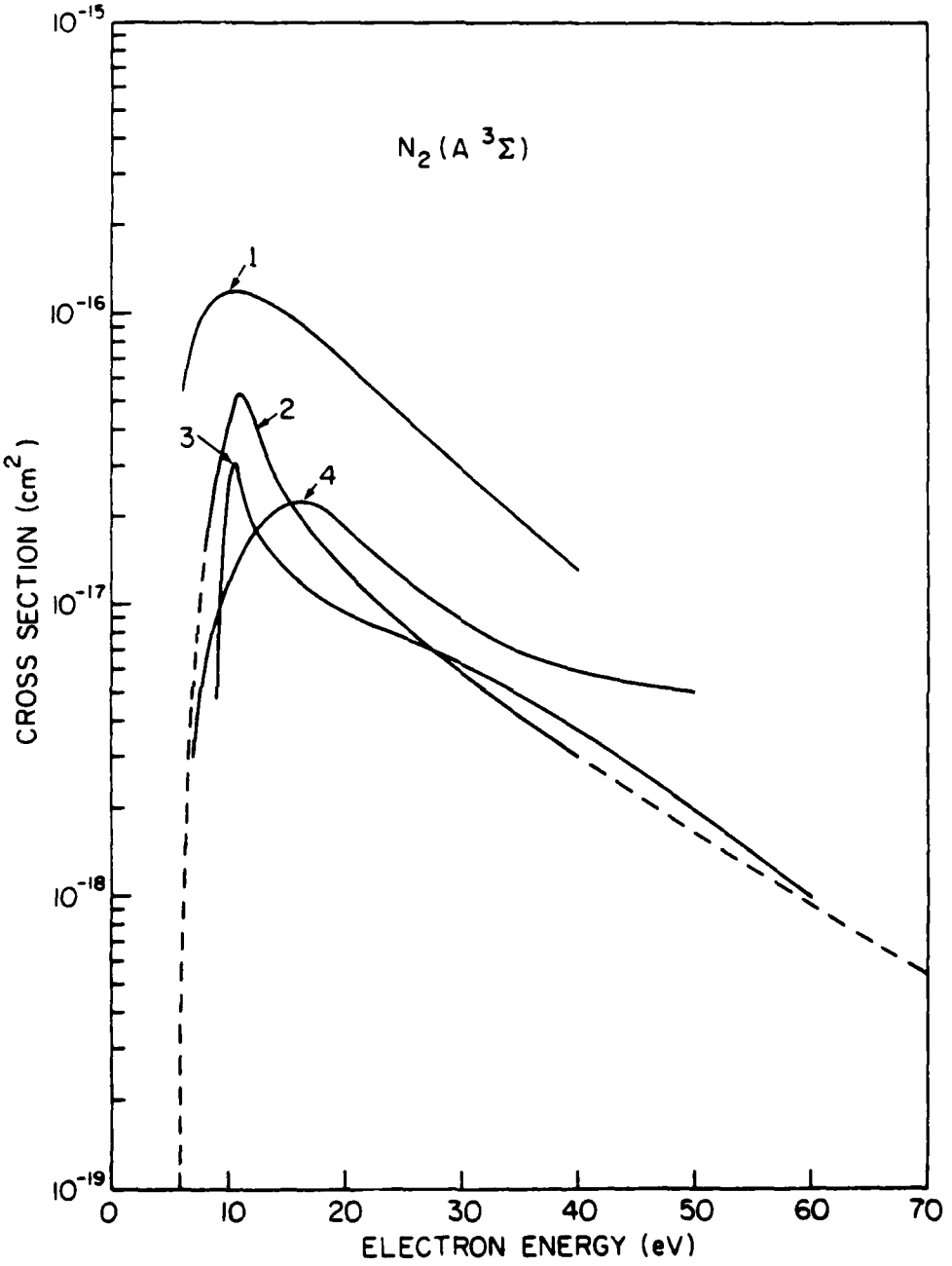

Fig. 5 — The Electron Impact Excitation Cross Section of $N_2(A^3\Sigma)$. For details see Ref. (7).

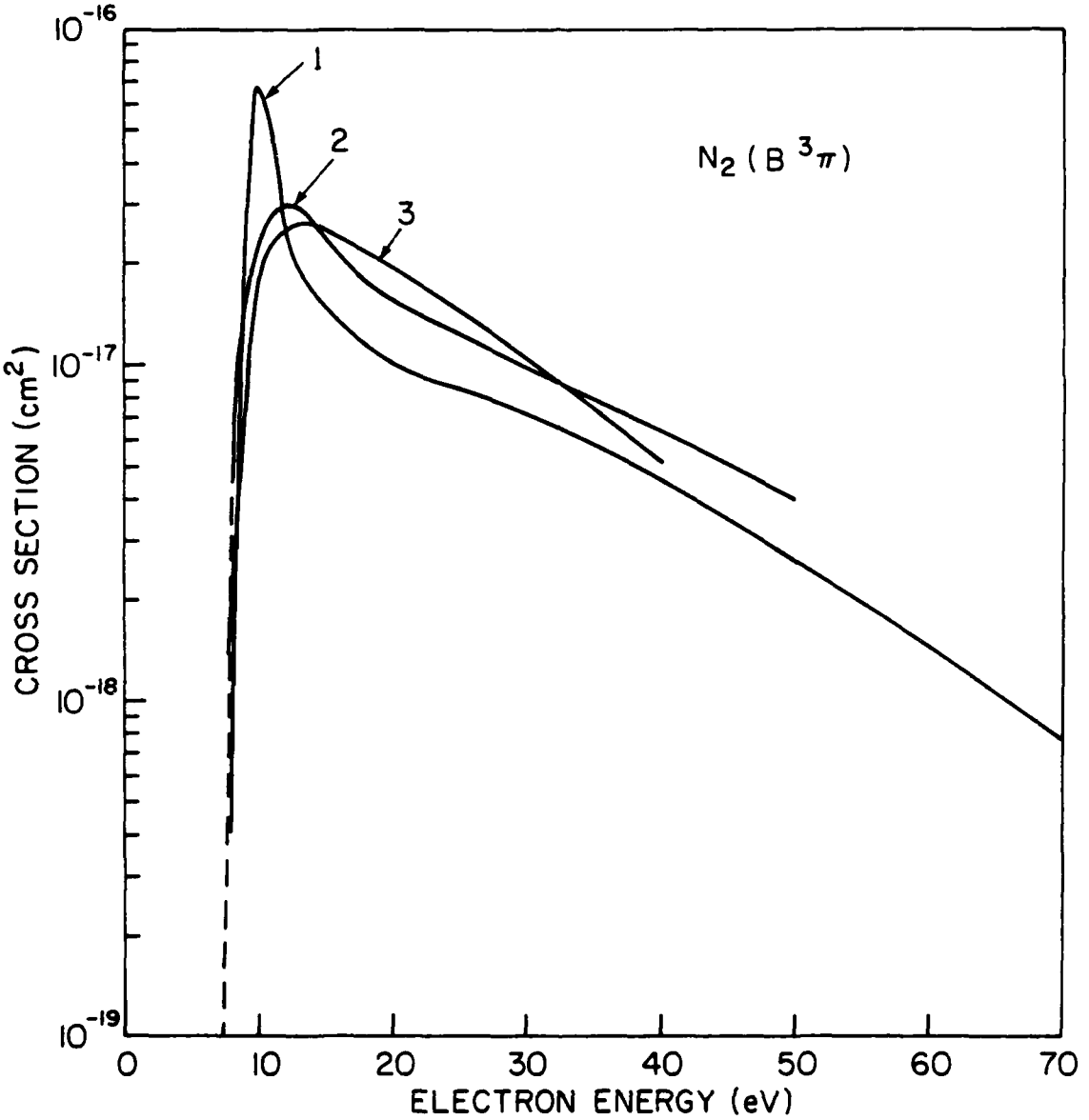

Fig. 6 — The Electron Impact Excitation Cross Section of $N_2(B^3\Pi)$. For details see Ref. (7).

TABLE 2

Relatively Strong Emissions in the Second Positive Band System

Wavelength (Å)	Transition (ν', ν'')	Wavelength (Å)	Transition (ν', ν'')
4059	0, 3	3755	1, 3
3998	1, 4	3710	2, 4
3943	2, 5	3577	0, 1
3894	3, 6	3536	1, 2
3804	0, 2	3371	0, 0
		3159	1, 0
		3163	2, 1

The lifetimes of these transitions are[20] in the range of tens of nanoseconds to fractions of a microsecond. Those vibrational levels are quenched by N_2 where the rate coefficient for the quenching of the (0, 0) transition is[21] 1.15×10^{-11} cm^3/sec.

The electron impact excitation cross section for the second positive band system has been calculated and measured extensively,[7] especially the cross section for the excitation of the (0, 0) transition at 3371 Å. The excitation cross section is shown in Figure 7.

$N_2^+(B)$: The nitrogen molecule has several ionization continua where upon the ionization the molecular ion is in an excited state. These are $N_2^+(A)$, $N_2^+(B)$, $N_2^+(C)$, etc. The $N_2^+(B)$ state has an ionization threshold of 18.8 eV and is the upper level for the first negative band system, N_2^+ ($B^2\Sigma \rightarrow X^2\Sigma$). The strong[18] emissions from this band system are given in Table 3.

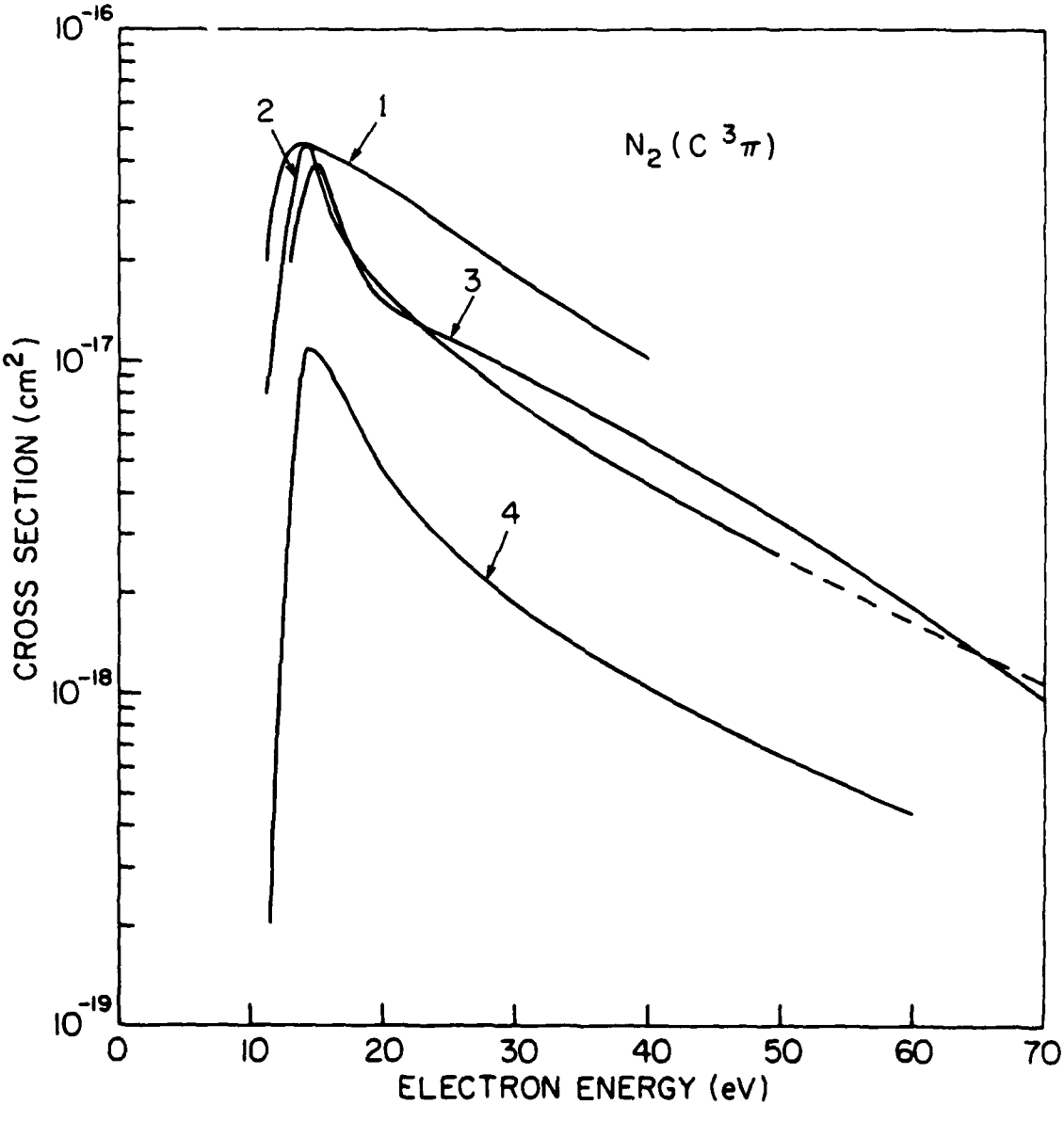

Fig. 7 — The Electron Impact Excitation Cross Section of $N_2(C^3\Pi)$. For details see Ref. (7).

TABLE 3

Relatively Strong Emissions in the First Negative Band System

Wavelength (Å)	Transition (ν', ν'')	Wavelength (Å)	Transition (ν', ν'')
5228	0, 3	4236	(1, 2)
5076	2, 5	3914	(0, 0)
4709	0, 2		
4599	2, 4		
4515	4, 6		
4278	0, 1		

The lifetimes of these states range[20] from tens of nanoseconds to microseconds and are quenched rapidly by N_2. The rate coefficient[22] for the quenching of the zeroth vibrational level is 4×10^{-10} cm^3/sec.

The fractional ionization leading to the $N_2^+(B)$ state is well established[7] for ionization by electrons with energy of 100 eV and higher. However, some data exist[23] for the fractional ionization below 100 eV, and emission cross section[24] which should be of more relevance to the ionization of N_2 by the microwave radiation.

$N(^2D)$: The metastable state of the nitrogen atom has an excitation energy[16] of 2.37 eV and arises by the dissociation of N_2, the dissociative recombination of N_2^+, and by direct electron impact excitation from the ground state of N. The electron impact excitation cross section of $N(^2D)$ has been calculated.[7]

3.4 GAS HEATING

One of the basic interests in the air breakdown is the heating of the plasma and the neutral species. The heating of the neutral species and the ions (since the collision between heavy particles is very efficient we assume that the ions and the neutrals have the same temperature) occurs through several atomic and molecular processes. These are: the elastic collisions of the electrons with the heavy particles, the quenching of the excited electronic states by the neutral species, the dissociative recombination of the molecular ions and the charge exchange process. The quenching of the vibrational energy through the collision between neutral species and vibrationally excited molecules is another essential source for the heating of the gas. However, the slowest heating rate among these various processes is the vibrational - translational energy exchange.

When the gas temperature rises, two additional ionization processes become operative. These are the thermal ionization and the associative ionization as expressed by Equations (20) and (21), respectively.

$$N_2 + N_2 \rightarrow N_2^+ + N_2 + e \quad (20)$$

$$N + N \rightarrow N_2^+ + e \quad (21)$$

4. APPLICATIONS TO BREAKDOWN STUDIES

There exist considerable experimental[25,26] data on the microwave breakdown in air and other gaseous elements. With the advent of lasers, the air breakdown studies at optical frequencies have increased considerably.[27-29] Theoretical calculations for the air, or gas breakdown generally proceed from the Boltzman's equation which is solved self consistently for the electron energy and its distribution. Analytical methods[26,27,30] are also utilized to obtain the breakdown threshold power. In this report we have assumed a maxwellian electron velocity distribution in our codes (we are planning to develop a Boltzman code for this purpose) and have utilized the code for the breakdown calculations.

4.1 MICROWAVE BREAKDOWN IN N_2

In order to compare our results with experiments, we have incorporated the effect of diffusion into the code. Thus we define an effective ionization rate $\nu_{ei} = \nu_i - D\,\Lambda^{-2}$ to allow for diffusion in our code. The diffusion is assumed to be free with a diffusion coefficient $D \simeq V_e^2\, t_c^2 \simeq 5 \times 10^{15}\, T_e$. The time $t_c = 1/\nu_c$ is the electron-neutral (electron-ion) collision time and V_e is the electron thermal velocity. The diffusion length Λ is regarded as being specified by the cavity and is assumed known. Our definition of breakdown is defined as the electric field required to achieve a <u>net</u> increase in the electron density for a ten nanosecond pulse. Once the cascade process begins, the electron density quickly reaches the critical density. The dominant loss processes at low and high pressures ($P \geq 1$ Torr) are diffusion and dissociative recombination ($N_4^+ + e \rightarrow N_2 + N_2$), respectively. Our comparison will be to experimentally measure cw breakdown in nitrogen. The criterion for cw breakdown in nitrogen is $\nu_i = \nu_r + D/\Lambda^2$ where ν_r is the dissociative recombination rate[31], $\nu_r = 5.0 \times 10^{-8}\, N_4^+/T_e$, where T_e is in eV. Both the diffusion length Λ and the ambient electron density ($n_0 = 10^2$ cm^{-3}) were specified in the experiment and are known parameters in our calculation.

Calculations were performed for various frequencies, diffusion lengths, and pressures. Figure (8) shows the results obtained by MacDonald et al.[26] for cw breakdown fields in nitrogen at frequencies 992MH and 9.4GH with diffusion lengths of 0.631 cm and 0.4 cm, respectively. The stars in Figure (8) denote the calculated breakdown threshold intensity using N_2-Chem. The calculated thresholds are higher as expected for pulsed breakdown. Table 4 shows the electron temperature, breakdown intensity, and characteristic time for electron production $\tau \equiv N_e \, (dN_e/dt)^{-1}$ as a function of the background pressure at f = 922 MH and Λ = 0.631 cm.

Table 4

Pulse Breakdown Threshold Power for 10 cm Wavelength for Various Nitrogen Pressures

Neutral density (cm^{-3})	Electron Temperature (eV)	Pulse Breakdown Power ($Watts/cm^2$)	τ (sec)
1.32×10^{18}	1.7	2200.	7.1×10^{-7}
1.32×10^{17}	2.4	80.	4.3×10^{-7}
1.32×10^{16}	6.4	60.	2.5×10^{-7}
1.32×10^{15}	41.0	153.	3.7×10^{-8}

The characteristic time τ represents roughly the maximum growth time for the electrons at the start of the avalanche process. Experiments show that once the pulse length $t_p \geq 25\mu s$, the pulse breakdown threshold approaches the cw breakdown limit. The generation time is approximately $t_g = \tau \log 2$ and we require 20 - 25 generations to reach electron densities of order $N_e \sim 10^{11}$ cm^{-3}. Again our definition of the breakdown power is the intensity required to achieve a net increase in the electron density in 10 ns. Therefore, our results are certainly applicable to pulse breakdown when $t_g \ll 25\mu s$. Since this is easily satisfied by our results, we would expect the higher breakdown field as characteristic of pulse breakdown. The high electron temperature at low pressure results from the strong diffusive losses. The agreement at lower pressures may be somewhat fortuitous since we extrapolate the ionization and excitation rates to energies above 20 eV. Current rate coefficients in the code are tabulated for T_e up to 20 eV.

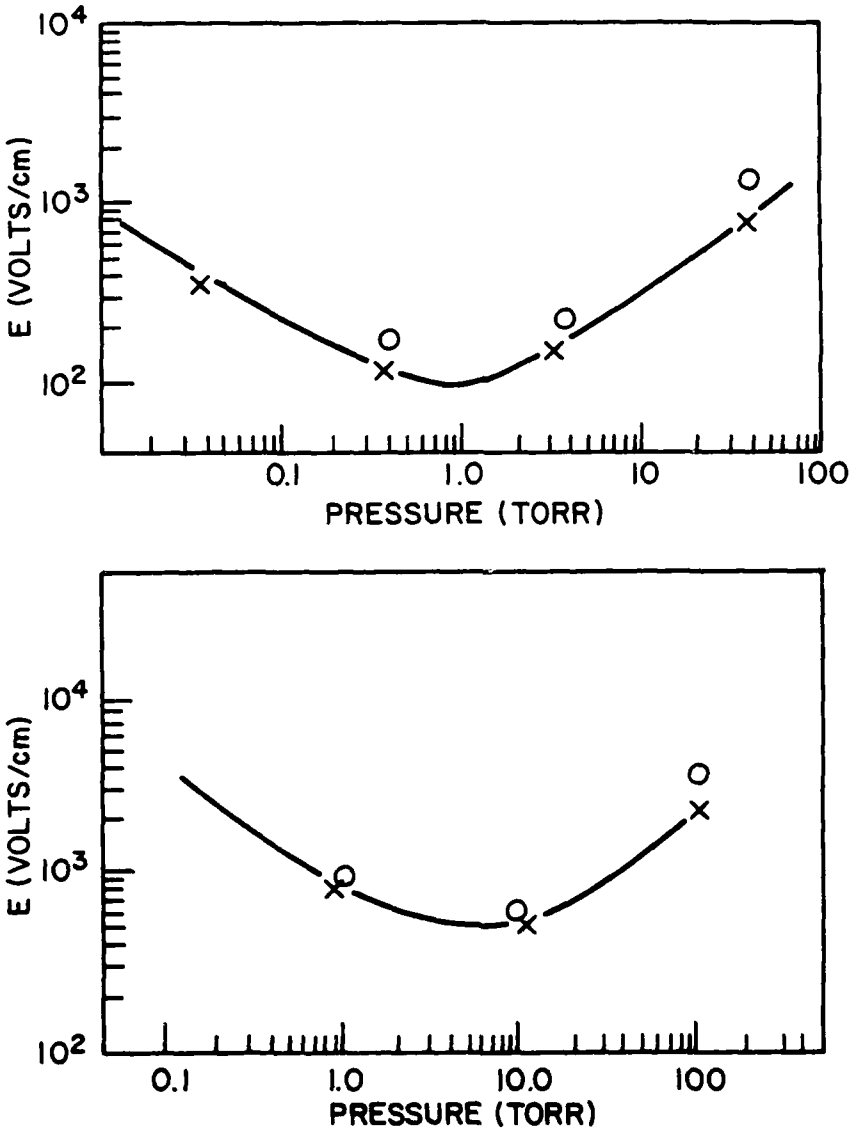

Fig. 8 — Comparison between experimental CW N_2 breakdown threshold power and calculations using the N_2 chemistry code, CHEMN2. Calculations are indicated by circles and crosses for pulsed and CW breakdown fields, respectively.

However, data is available for T_e above this temperature and will be incorporated into the code if desired.

4.2 MICROWAVE AIR BREAKDOWN OFF A REFLECTING SURFACE

We have also coupled the E and M code to a detailed air chemistry code[32] (CHMAIR) to study the breakdown in air. We have, however, chosen to calculate the breakdown off a reflecting surface to illustrate the breakdown in air as a result of the interference between the incident and the reflected waves. In these calculations we neglect the hydrodynamic effects and assume that chemical processes are more effective in depleting the electron density than diffusion. This is especially true in microwave absorption experiments with short pulses ($t_p \leq 40$ ns) and rather long wavelength radiation conducted at atmospheric pressures. Assuming the diffusion length $\Lambda \simeq \lambda$, at atmospheric condition the characteristic electron diffusion time, for 10 cm radiation, is roughly $t_D \simeq (\Lambda/L_{mfp})^2 t_c \simeq 10^{-7}$ sec where L_{mfp} is the mean free path of the electron. Since the diffusion time $t_D \gg t_p \simeq 40$ns, our neglect of hydrodynamic effect would seem a good assumption.

The intensity of the standing wave patterns resulting from the interference maximum can easily be above the threshold for air breakdown. We imagine the microwave to be incident on a reflecting surface with intensity $I_0 < I_B$. At the first maximum (one-quarter wavelength from the surface) the field intensity is $I = 4\ I_0$ with air breakdown commencing rapidly a distance $\frac{\lambda}{4}$ from the surface (Figure 9a). Figure 9b shows the rapid increase of the electron density as the avalanche begins. The extreme sensitivity of the air breakdown to the electric field essentially localizes the electron density resulting in sharp scale lengths, $L = N_e\ (dN_e/dy)^{-1} < \lambda$. In this simulation, we have a pulse of 10cm wavelength radiation incident normal to a reflecting surface with an intensity of $I_0 = 0.5 MW/cm^2$ and a pulse duration of 40ns. The initial ambient electron density is taken to be $n_0 = 10 cm^{-3}$ at standard temperature and pressure (STP).

In a collisional plasma, $\nu_c \gg \omega$, the cut off density for propagation of electromagnetic radiation is not sharply defined as in collisionless plasmas. At sufficiently high density such that the skin depth $\delta \leq \lambda$, the breakdown region closest to the surface is decoupled from the microwave radiation. This is seen in Figure 10a, where we show the square of the electric field at the end of a 40ns pulse. In this particular simulation, we allow for multiple sources (each source below threshold) such that the net intensity

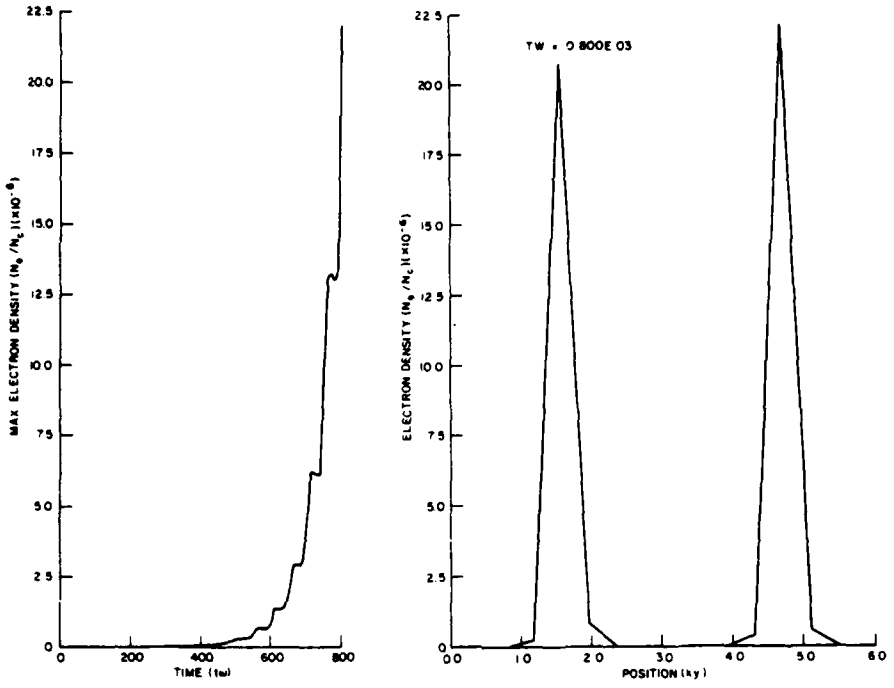

Fig. 9 — (a) Air breakdown off a reflecting surface at atmospheric conditions with incident power I = 0.5MW/cm^2 at λ = 10 cm. (b) Time development of the electron density (N_e/N_c).

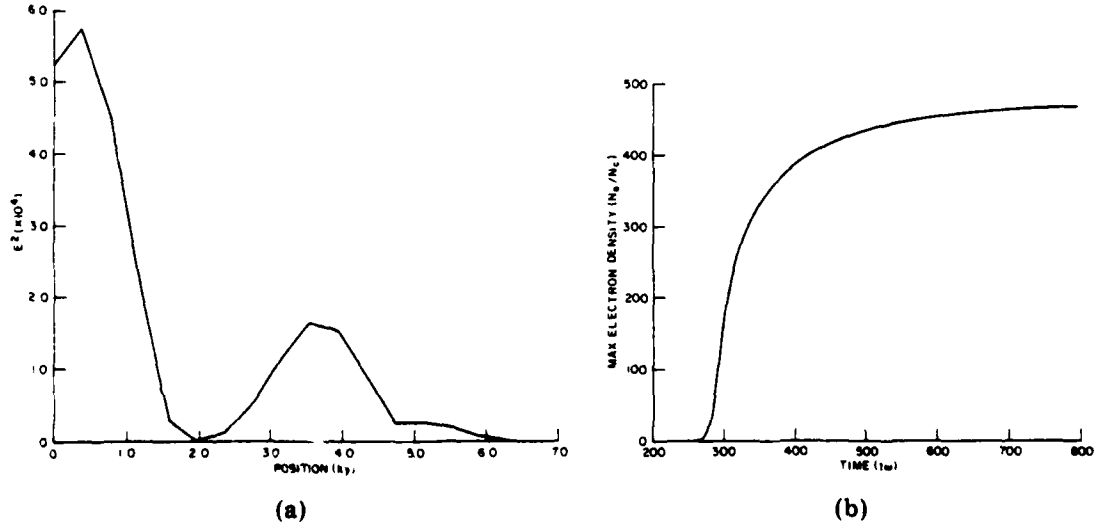

Fig. 10 — (a) The square of the electric field at the end of the pulse for t_p = 40 nsec. (b) Time development of the electron density (N_e/N_c).

$I_0 = 2MW/cm^3 > I_B$. The corresponding density for $\delta < \lambda$ can be easily calculated to be $N_e \simeq 500N_c$. Figure 10b shows the time history of the rise of the electron density to $N_e \leq 500N_c$. Though air breakdown is occurring throughout the volume for this particular simulation, the extreme sensitivity of the air breakdown to the electric field again localizes the region of the electron density. The important point to be made here is the high electron density. As will be shown later, the reflection coefficient for an idealized sharp electron density profile is insignificant until $N_e \simeq 10^5 N_c$ at $\lambda = 10cm$. The high electron density makes real the possibility of driving a hydrodynamic response with microwaves, pending the inclusion of the hydrodynamic effects and various pulse shapes and pulse lengths. Early work by Wood[33] using the hydrodynamic code LASNEX suggests the formation of shocks at atmospheric conditions using microwave radiation.

4.3 REFLECTION OF MICROWAVE RADIATION

Once the electron density becomes sufficiently large $N_e >> N_c$, the plasma becomes a good absorber of microwave radiation. However, at too high densities, the plasma becomes a good reflector of microwave. We wish to obtain maximum bounds on the reflection and absorption coefficient of the plasma as a function of wavelength and electron density. We proceed further by calculating the absorption and reflection coefficient for an idealized slab density profile of density N and thickness d (See Figure 11). We consider multiple reflection and vary the wavelength, density, and thickness of the microwave plasma system. In particular we examine the reflection at two microwave frequency of 3GH and 30GH, respectively. The electron-neutral collision frequency is assumed to be $\nu_c = 5 \times 10^{12}$ sec^{-1} which is typical at ambient atmospheric conditions. The reflection and transmission coefficients are given by

$$R = \left| \frac{E_{ref}}{E_{inc}} \right| = \left| \frac{S\ (1 - e^{-i\epsilon})}{1 - S^2\, e^{-i\epsilon}} \right|^2$$

and

$$T = \left| \frac{E_{Trans}}{E_{inc}} \right|^2 = \left| \frac{(1 - S^2)\, e^{-i\epsilon/2}}{1 - S^2\, e^{-i\epsilon}} \right|^2$$

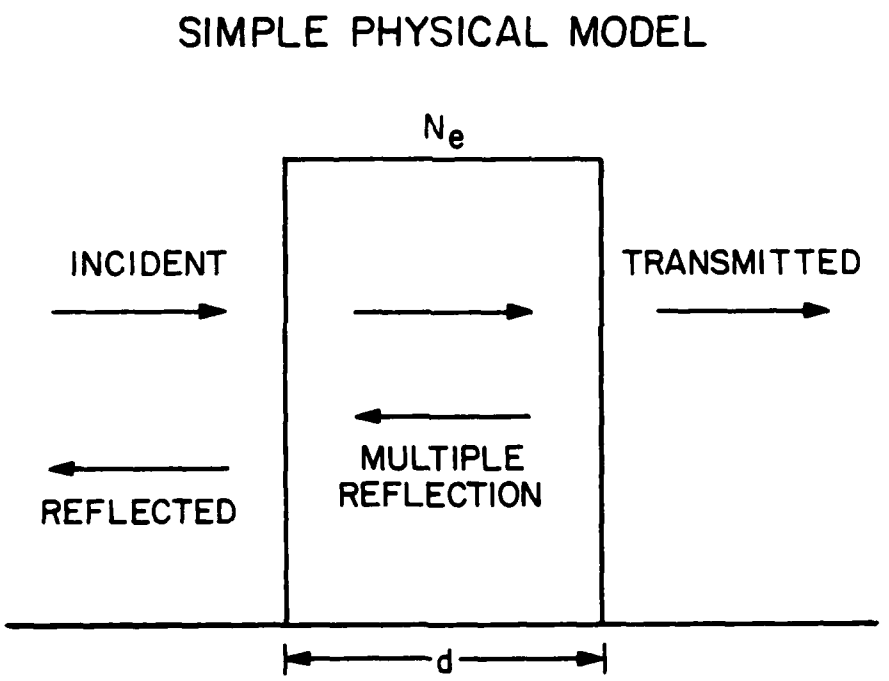

Fig. 11 — The idealized slab density profile is characteristic of systems with high electron densities and steep density profiles.

where $S = (1 - n)/(1 + n)$ and $\epsilon = 2n\omega d/c$. The complex refraction index $n = n_r - in_i$ is

$$n_r = \left\{ \frac{(1 - a)}{2} \left[1 + \sqrt{1 + \frac{4b^2}{(1 - a)^2}} \right] \right\}^{\frac{1}{2}}$$

$$n_i = \left\{ \frac{(1 - a)}{2} \left[1 + \sqrt{1 + \frac{4b^2}{(1 - a)^2}} \right] \right\}^{\frac{1}{2}}$$

when $1 - a > 0$ and

$$n_r = \left\{ \frac{(a - 1)}{2} \left[\sqrt{1 + \frac{4b^2}{(a - 1)^2}} - 1 \right] \right\}^{\frac{1}{2}}$$

$$n_i = \left\{ \frac{(a - 1)}{2} \left[\sqrt{1 + \frac{4b^2}{(a - 1)^2}} + 1 \right] \right\}^{\frac{1}{2}}$$

when $1 - a < 0$, where $a = \frac{\omega_p^2}{(\omega^2 + \nu_c^2)}$ and $b = \frac{\nu_c a}{2\omega}$.

The absorption is determined by the condition $R + T + A = 1$ with the thickness measured in units of the skin depth δ, $\delta k = \frac{1}{n_i}$. Since the results for $d = \delta$ and $d \gg \delta$ are somewhat similar, we present the results only for $d \gg \delta$.

Figure 12 shows the reflection and absorption coefficients, as a function of plasma density at $\lambda = 10$cm and $\lambda = 1$cm light, respectively. If we assume an absolute electron density of $N_e = 10^{15}cm^{-3}$, we see the reflection coefficient is roughly 60% for 10cm light ($N_e = 10^4 N_c$). Whereas, for 1cm light, the reflection coefficient is approximately 25% at $N_e = 10^{15}cm^{-3} = 10^2 N_c$. Our calculations also indicate that to maintain a plasma density of $N_e = 10^{15}cm^{-3}$ requires an absorbed power of $I_{abs} \simeq 0.8MW/cm^2$. Using a 10cm light would require an incident power level of $I_{inc} \geq 1.6MW/cm^2 > I_B$. Obviously, once the incident power is above the breakdown threshold, the

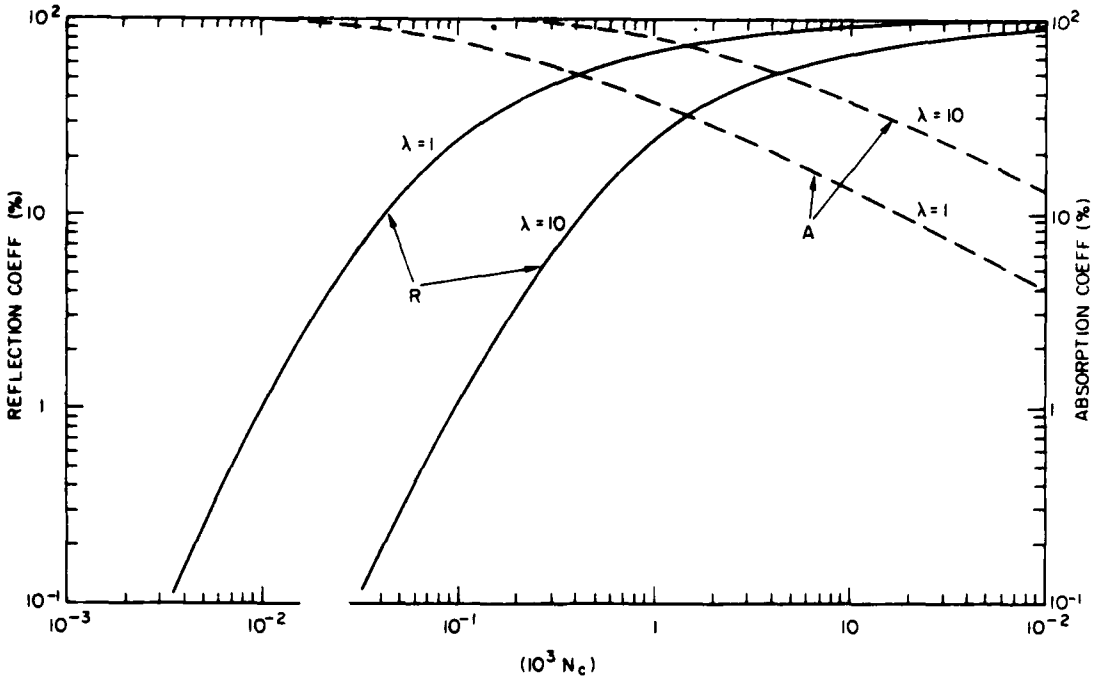

Fig. 12 — Reflection and absorption coefficient as a function of the electron density in the slab plasma model with $\nu_c = 5 \times 10^{12}$ sec^{-1}.

plasma would be impossible to maintain. However, the prospects of maintaining a plasma at $N_e = 10^{15}cm^{-3}$ using a 1cm light appears feasible since an incident intensity of $I_{inc} \simeq 1MW/cm^2 < I_B$ would only be required. Though the electron density $N_e \simeq 10^{15}cm^{-3}$ is clearly arbitrary, it is not unreasonable to expect the plasma to become a good reflector when $\omega_p^2 \geq \nu_c^2 + \omega^2$.

5. Conclusions

We have presented and discussed two codes developed for the studies of the pulsed microwave interaction with N_2. We have also utilized our E and M code coupled to a chemistry code to study the breakdown in air. Our breakdown threshold power calculations agree favorably with experimental data in N_2.

Our calculations for breakdown near a surface brings forth the importance of reflection from a plasma on its maintenance and heating. However, additional studies in this subject are in progress to delineate this point further, including the hydrodynamic effects.

REFERENCES

1. V. L. Ginzburg, "Propagation of Electromagnetic Waves in Plasma", Pergamon Press, Oxford (1964).
2. E. L. Lindman, J. Computational Phys. 18, 66 (1975).
3. R. D. Richtmyer and K. W. Morton, "Difference Method for Initial Value Problems", J. Wiley, New York (1967).
4. R. N. Varney, Phys. Rev. 89, 708 (1953), ibid 174, 165 (1968) and references therein.
5. J. L. McCrumb and P. Warneck, J. Chem. Phys. 66, 5416 (1977).
6. A. G. Englehardt, A. V. Phelps and C. G. Risk, Phys. Rev. 135, A1566 (1964).
7. A. W. Ali, "Excitation and Ionization Cross Sections for Electron and Microwave Energy Depositions in Air", NRL Memo Report 4598 (1981).
8. G. J. Schultz, Phys. Rev. 135, A988 (1964) and references therein.
9. D. Spence, J. L. Maurer and G. J. Schulz, J. Chem, Phys. 57, 5516 (1972).
10. H. Eherhard and K. Willman, Zeit, Phy. 204, 462 (1967).
11. D. Rapp and P. Englander-Golden, J. Chem, Phys. 43, 1464 (1965).
12. H. F. Winters, J. Chem, Phys. 44, 1472 (1966).
13. E. C. Zipf and R. W. McLaughlin, Planet Space Sci. 26, 449 (1978).
14. A. W. Ali, "The Physics and the Chemistry of Two NRL Codes for the Disturbed E and F Regions", NRL Report 7578 (1973).
15. A. W. Ali, "The Physics and the Chemistry of NRL Master Code for the Disturbed E and F Regions", NRL Memo Report 3732 (1978).
16. A. W. Ali, R. H. Kummler, F. R. Gilmore and J. William McGowan, "Upper Atmospheric Excitation Processes", NRL Memorandum Report 3920 (1979).
17. V. I. Kuklin, A. P. Osipov and Y. M. Chuvilskii, Soviet Physics, Tech. Phys. 24, 883 (1980).
18. R. W. B. Pearse and A. G. Gaydon, "The Identification of Molecular Spectra", Chapman and Hall, London (1965).
19. D. C. Cartwright, J. Geophys. Res. 83, 517 (1978).
20. R. W. Nicholls, Annals de Geophys. 20, 144 (1964).
21. P. Millet, Y. Salamero, H. Brunet, J. Galy, D. Blanc and J. L. Teyssier, J. Chem. Phys. 58, 5839 (1973).
22. M. N. Hirsh, E. Poss and P. N. Eisner, Phys. Rev. A1, 1615 (1970) and references therein.

23. G. R. Wight, M. J. Van der Wiel and C. E. Brion J. Phys. B. Atom. Mol. Phys. 9, 675 (1976).

24. J. W. McConkey, J. M. Woolsey and D. J. Burns, Planet Space Sci. 15, 1332 (1967).

25. M. A. Herlin, and S. C. Brown, Phys. Rev. 74, 291 (1948).

26. A. D. MacDonald, D. V. Gaskell and H. N. Gitterman, Phys. Rev. 130, 1841 (1963).

27. See e.g. C. Demichelis, IEEE, J. Quantum. Electron, QE-5, 188 (1969) and references therein.

28. N. Krall and K Watson, Phys. Rev. A5, 1883 (1972).

29. Y. P. Raizer, "Laser-Induced Discharge Phenomena", Consultants Bureau, New York (1977).

30. A. W. Ali, "The Microwave Application Theory Program at NRL and Some Chemistry Code Applications to Ionospheric Heating by Microwave Radiation", NRL Memo Report 4302 (1980).

31. M. A. Biondi, Chapter 16, Defense Nuclear Agency Reaction Rate Handbook, DNA 1948 H., Bortner and Baurer Eds., DASIAC, DoD Nuclear Information and Analysis Center, GE-Temp, Santa Barbor, Ca. (1972).

32. R. F. Fernsler, A. W. Ali, J. R. Greig and I. M. Vitkovitsky, NRL Memo Report 4110 (1979).

33. C. H. Wood, Bull Am Phys. Sci 25, 909 (1980).

DISTRIBUTION LIST

DIRECTOR
Defense Advanced Research Project Agency
Architect Building
1400 Wilson Blvd.
Arlington, VA. 22209
ATTN: Strategic Tech. Office
Dr. J. Bayless
Dr. J. Mangano

Defense Technical Information Center
Cameron Station
Alexandria, VA. 22314
ATTN: TC — 2 copies

DIRECTOR
Defense Intelligence Agency
Washington, DC 20301
ATTN: W. Wittig DC - 7D
DT-1B
P. Castleberry

B-K Dynamics, Inc.
15825 Shady Grove Rd.
Rockville, MD. 20850
ATTN: Mr. I Kuhn

CHIEF OF Naval Research
Department of the Navy
Arlington, VA. 22217
ATTN: Code 464, T. Berlincourt
Code 421, Dr. W. J. Condell

COMMANDING OFFICER
Naval Research Laboratory
Washington, DC. 20375
ATTN: Code 4701, Jack D. Brown
Code 4700, Division Superintendent — 26 copies
Code 4700.1 Dr A W. Ali — 50 copies
Code 4777 Mr. I. M. Vitkovitsky
Code 4790 Dr. M. Lampe
Code 4740, Dr. V. Granatstein
Code 6805, Dr. R. Parker
Code 6330, Dr. T. J. Schriempf
Code 4790, Dr. W. Manheimer
Code 4704, Dr. C. Roberson

COMMANDER
Naval Surface Weapons Center
White Oak, Silver Spring MD. 20910
ATTN: Code 1224 Navy Nuc Programs Office
Code 730, Tech. Lib.
Dr. C. M. Huddleston

AF Weapons Laboratory, AFSC
Kitland AFB NM 87117
ATTN: Maj. H. Dogliani
Dr. K. Dreyer
Lt. David L Smith
Dr. D. Straw

AFTAC
Patrick AFB, FL. 32925
ATTN: TF Maj. E. Hines
TF Capt. Wiley
TN

HQ USAF/RD
Washington, DC. 20330
ATTN: RDQ

University of California
Lawrence Livermore National Laboratory
P O Box 808
Livermore, CA. 94550
ATTN: Tech Info Dept L-3
C. H. Wood

Naval Air Systems Command
Jefferson Plaza #1
Washington, DC. 20361
ATTN: Dr. R. Wasneski

Sandia National Laboratory
P.O. Box 5800
Albuquerque, NM. 87185
ATTN: R. B. Miller

Science Applications, Inc.
5 Palo Alto Square
Palo Alto, CA. 94304
ATTN: Dr. R. Johnston

COMMANDER
U.S. Army Missile Command
Redstone Arsenal
Huntsville, AL. 35809
ATTN: AMSMI-YTT W. G. Preussel, Jr.
P. Oliver

Mission Research Corporation
5503 Cherokee Ave.
Alexandria, VA. 22304
ATTN: Dr. C. Yee
Dr. M. Bollen

Office of Naval Material
Office of Naval Technology
Washington, DC. 20360
ATTN: Dr. J. Kershenstein

DIRECTOR
Defense Nuclear Agency
Washington, DC.
ATTN: Dr. C. Fitz (RAAE)
Dr. P. Lunn (RAAE)

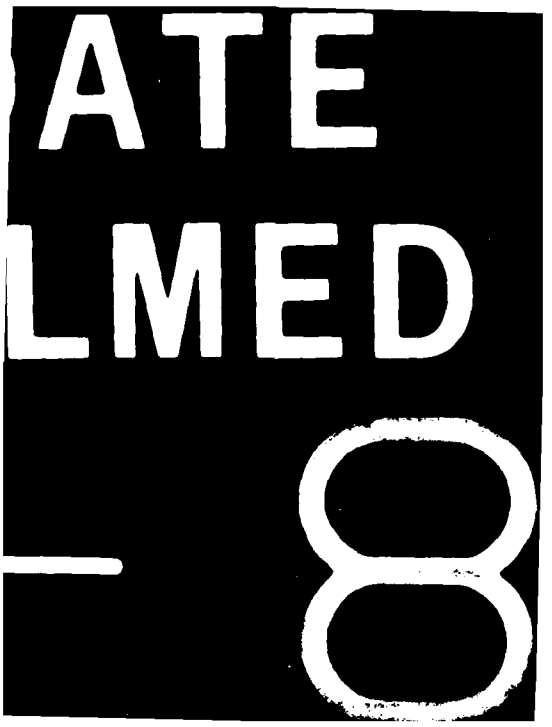
ATE
LMED
8